Augmented Gaussian-orbital basis for atomic-cluster calculations within the density-functional formalism: Application to Cu_2

G. S. Painter and F. W. Averill*
Metals and Ceramics Division, Oak Ridge National Laboratory, Oak Ridge, Tennessee 37831
(Received 13 June 1983)

The principle of augmentation, used to introduce inner-atom core structure into slowly varying basis functions, is applied to Gaussian orbitals to define a new basis set for highly accurate total-energy calculations for atomic clusters within the density-functional formalism. Diffuse Gaussian-orbital tails are matched continuously and differentiably to inner-atom numeric radial functions at the atomic-sphere radius. Major advantages of Gaussian-orbital basis sets are acquired without the need for numerous Gaussians of large exponent for the core region. The numeric functions used inside the atom permit essentially exact solutions for that region. Procedures are described which recover use of the efficient integral algorithms for the Gaussian-orbital-tail matrix elements. The interactions over the structured inner-atom region are treated by efficient integrand smoothing and integration procedures for the sphere. The new augmented Gaussian basis removes the primary limitations on the use of Gaussian orbitals for heavy atoms. As an illustration the method is applied to the copper dimer in an all-electron framework within the local-spin-density approximation (LSDA). The calculated binding energy, equilibrium separation, and first ionization potential of Cu_2 are within 2% of experiment within the $X\alpha$ model. Excitation energies are better described within more recent refined exchange-correlation functionals. These all-electron results show the LSDA model predicts a slightly contracted bond length for Cu_2, consistent with bulk LSDA calculations for the $3d$ transition-metal series.

I. INTRODUCTION

Among *ab initio* Hartree-Fock and configuration-interaction (CI) calculations for finite atomic clusters, by far the majority are formulated in terms of Gaussian-type-orbital (GTO) basis sets. The motivating factor for this choice is the existence of explicit formulas for the basic integrals of the secular matrix.[1] A limitation on the use of Gaussians for heavy atoms is the large number of primitive Gaussians required to describe the rapidly varying orbital structure in the core region. Indeed it has been pointed out[2] that focus on this problem has often been to the detriment of the description of the valence states. The accentuation of this difficulty for atoms of the transition-metal series has led to new efforts to improve all-Gaussian basis sets.[3] An alternate way of dealing with the basis size problem replaces the core part of the basis by a pseudopotential, as exemplified in the calculations on Cu_2 carried out by Pelissier.[4]

The use of GTO basis sets within the local-spin-density approximation[5] (LSDA) has lagged these developments in the quantum-chemical field. Following their introduction[6] for first-principles band-structure calculations numerous GTO studies[7] have been carried out. The use of GTO basis sets in local-density molecular calculations was initiated in the work by Sambe and Felton.[8] With refinements introduced by Dunlap and co-workers,[9] particularly with variational fit procedures, the GTO method has provided reliable spectroscopic constants in a number of $X\alpha$ calculations. The GTO approach has also been used in local-density calculations[10] with all matrix elements evaluated by Gaussian integral algorithms[11] without invoking charge or potential fits.

Evaluation of the Coulomb energy due to the interelectronic repulsion remains the rate-determining step in all current linear variational methods, regardless of basis, just as the multicenter r_{12}^{-1} matrix elements have been the major problem in *ab initio* calculations. With Gaussian orbitals, electron repulsion matrix elements can be obtained in integral form, and this is the major motivation for adopting the basis. But only the overlaps among diffuse orbital tails pose any difficulty; in the LSDA the intrasite terms can be efficiently treated by alternate means. Thus retention of a Gaussian representation for the orbital description inside the atom becomes a liability in the LSDA. Numerical radial functions,[12,13] however, are known to be near optimum for spanning the inner-atomic region.

In the present approach, a partitioned basis set is introduced to optimize both the orbital description over all space and the treatment of resulting matrix elements. Diffuse Gaussians are used to span the interstitial volume, and numerical-radial functions are used for the orbital expansion in the nominal atomic-sphere region (a representation which permits an exact description of the core wave functions). Rather than continuing the numerical orbital form outside the atomic spheres, as in various linear combinations of atomic orbital (LCAO) methods,[12] each (valence) function is matched (along with higher derivatives) to a sum of diffuse Gaussian functions at the sphere boundary. This is much in the spirit of the linear combination of muffin-tin orbitals (LCMTO) approach,[13,14] especially more recent variations[15–17] where the nonlinear

parameters determining the form of the Hankel-function "tail" are selected to give atomiclike behavior to the basis function about its defining site.

From similarities to band-structure methods wherein slowly varying interstitial basis functions are augmented by numeric functions inside the atomic spheres (e.g., augmented plane wave,[18] spherical wave,[19] and Gaussian wave[20]), this set of localized functions will be referred to as an augmented Gaussian basis (AGB). The concept of augmentation is basic to the majority of new techniques for carrying out local-density calculations. The main purpose here is to combine it with the advantageous characteristics of Gaussian orbitals in order to facilitate treatment of clusters involving heavy (transition-metal) atoms. Though not as simple as the pseudopotential method, the augmentation procedure as used here is an all-electron method (the frozen-core approximation is not evoked) thus allowing a wider class of systems to be addressed reliably. Since the choice of Gaussian-orbital tails for the basis functions outside the spheres permits the use of explicit formulas for the evaluation of most matrix elements, a major part of the calculation can be carried out essentially analytically. Equally important is the characteristic of reliability guaranteed by the Gaussian basis. Simple procedures, such as "freeing" the most diffuse Gaussian in each l channel, give excellent convergence properties.[21] This provides a basis-extension procedure which is both systematic and reliable, and avoids many of the problems associated with alternate basis sets.

II. AUGMENTED GAUSSIAN ORBITAL BASIS SET

The augmented Gaussian orbitals are defined in a spatially partitioned form by Eq. (1):

$$\chi_j(\alpha,\vec{r})=\begin{cases}\Phi_j(\vec{r}_j), & |\vec{r}_j|\le R_0^j \\ G_j(\alpha,\vec{r}_j), & |\vec{r}_j|\ge R_0^j\ .\end{cases} \tag{1}$$

Here $\vec{r}_j=\vec{r}-\vec{R}_j$ is the vector specifying a point at $\vec{r}$ relative to the defining site j which is located at $\vec{R}_j$, and R_0^j is the nominal radius of the atom at site j. The orbital form inside the sphere is simply (now taking $\vec{r}$ to denote the local $\vec{r}_j$)

$$\Phi_j(\vec{r})=\phi_j(r)Y_{l_jm_j}(\hat{r})\ . \tag{2}$$

Since this set must span the core region, a logical choice for the minimal basis portion of the basis set consists of the numerical solutions to the radial differential equation using the spherical component of the potential inside the spheres.[22] In Appendix A, an alternate form is described which makes a useful connection with other current linear combination of Gaussian-type orbitals (LCGTO) calculations. The atomic sphere introduced in defining the basis should not be taken to imply any shape approximation in the potential function. The spatial partitioning is only a construct used to gain calculational advantage. Most simply, a set of nonoverlapping spheres are defined (of equal or comparable volume) with the cluster in its configuration of smallest volume, and these radii are kept constant as the atoms are moved apart. Alternately, the sphere radii can be increased as the cluster expands. In practice, changing the sphere radii simply means calculational effort is shifted from one region to another.

The basis function outside the defining sphere (the orbital tail) is an expansion in Gaussian functions,[23]

$$G_j(\vec{r})=\left[\sum_i a_j^i\exp(-\alpha_i r^2)\right]r^{l_j}Y_{l_jm_j}(\hat{r})\ . \tag{3}$$

The linear coefficients for a given set of exponential parameters are determined by the match of the inside and outside functions and successive derivatives at the sphere radius. Optimization of the fit to $\phi_j(r)$ continued outside the sphere is obtained by varying the exponents (and recalculating the linear coefficients). In contrast to the LCMTO approach, no energy derivative function $\dot{\phi}$ is used, nor is matching of the Gaussian tail to inside functions at other sites carried out; rather the tails simply overlap other sites.[24] The task of the orbital tails is to provide adequate variational freedom in the valence space, and the definition for a minimal atomic basis has been given above. To supplement this set, free diffuse Gaussian tails can be included, just as in the usual LCGTO method, and the inside function corresponding to each is just the continuation of the tail into the defining sphere ($\phi_j\equiv G_j$, for $r\le R_j^0$).

For illustrative purposes an augmented Gaussian orbital χ representing the $4s$ orbital in copper is plotted in Fig. 1. The tail representation is also shown extended back to the defining-sphere origin. The effect of the augmentation procedure on the tail orbital is then apparent as the difference $(\chi-G)$ (nominal sphere radius ~ 1.8 a.u.). The corresponding kinetic energy-density contributions $r^2\nabla^2\chi$ and $r^2\nabla^2 G$ are illustrated for the same $4s$ AGB orbital in Fig. 2. From these figures it is clear that an advantage can be acquired if the rapidly varying parts of χ and $\nabla^2\chi$ inside the atomic spheres are dealt with separately from the

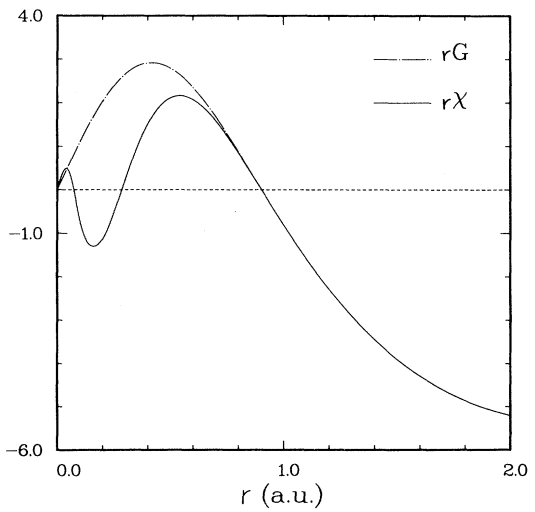

FIG. 1. Augmented Gaussian orbital, $r\chi$, representing $4s$ atomic orbital of copper. Orbital tail function, rG, is shown extended back to origin.

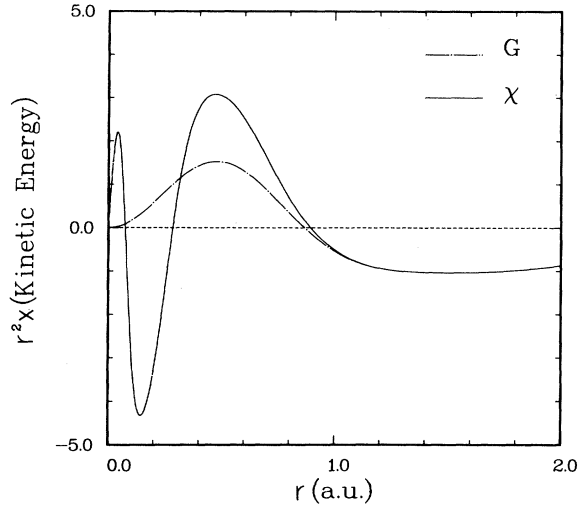

FIG. 2. Kinetic energy functions for copper 4*s* augmented Gaussian orbital, $r^2\nabla^2\chi$, and orbital tail, $r^2\nabla^2 G$, shown continued back to origin.

slowly varying parts G and $\nabla^2 G$. In Sec. II procedures are described which use this partitioned form of the AGB to gain advantages in matrix element evaluation.

III. MATRIX ELEMENTS

Evaluation of matrix elements of the Hamiltonian is carried out by first introducing a partitioning of space into nonoverlapping atomic spheres and the interstitial volume outside. If H represents an operator of the Hamiltonian then

$$\langle \chi_i \mid H \mid \chi_j \rangle_\infty = \langle G_i \mid H \mid G_j \rangle_{\Omega_I} + \sum_k \langle \chi_i \mid H \mid \chi_j \rangle_{\Omega_k} , \tag{4}$$

where subscript Ω_I denotes integration over the region outside the atomic spheres and subscript Ω_k integration over the kth sphere. Equation (4) simply breaks the integral over all space to show the explicit form for χ in the interstitial volume. Next, each Gaussian orbital G_i is continued into all the atomic spheres, the interstitial integral involving the Gaussians is extended to cover all space, and corrective terms are included for the overcounted contributions inside the spheres. Explicitly,

$$\langle \chi_i \mid H \mid \chi_j \rangle_\infty = \langle G_i \mid H \mid G_j \rangle_\infty + \sum_k (\langle \chi_i \mid H \mid \chi_j \rangle_{\Omega_k} - \langle G_i \mid H \mid G_j \rangle_{\Omega_k}) . \tag{5}$$

Note that the matrix element contribution from sphere k (in parentheses) is identically zero, unless the defining site of either χ_i or χ_j is sphere k. This simply reflects that there is no correction necessary for tail-tail overlap inside the spheres. On the other hand, the extension of the Gaussian tail into its *own* defining sphere invokes corrective terms of two sorts represented below by I_1 and I_2.

The correction integral

$$I_1 = \langle \Phi_i \mid H \mid \Phi_j \rangle_{\Omega_i} - \langle G_i \mid H \mid G_j \rangle_{\Omega_i} \tag{6}$$

treats the case where χ_i and χ_j are both centered on site i, and

$$I_2 = \langle \Phi_i \mid H \mid G_j \rangle_{\Omega_i} - \langle G_i \mid H \mid G_j \rangle_{\Omega_i} \tag{7}$$

is the proper correction when χ_i is centered on site i, which differs from site j. The first term in both Eqs. (6) and (7) clearly represents the correct matrix element contribution for sphere i, and the second term removes the overcounted contribution from the "global" integral $\langle G_i \mid H \mid G_j \rangle_\infty$.

The advantages of this procedure with regard to efficient matrix element evaluation are clear in that the difficult integral on the left-hand side of Eq. (5) has been replaced by a combination of simple integrals. For H representing most of the operators in the Hamiltonian, the global integral $\langle G_i \mid H \mid G_j \rangle_\infty$ is readily evaluated using integral alogrithms for Gaussian functions, and the remaining terms on the right-hand side of Eq. (5) are efficiently evaluated by standard procedures for the sphere. Writing the correction term for sphere k in the form

$$I = \int_{\Omega_k} (\chi_i H \chi_j - G_i H G_j) d\vec{r} , \tag{8}$$

a further nice property becomes apparent. As $r \to R_0^k$, the integrand uniformly goes to zero by construct of the basis, a characteristic which can be exploited to optimize the sphere integration.

When H represents the electronic Coulomb potential or exchange-correlation potential function, the integral algorithms for Gaussian functions cannot be directly applied, and special procedures described subsequently are used to evaluate the global integrals. The expressions for the matrix elements of the Hamiltonian are summarized in Appendix B.

IV. CHARGE DENSITY AND POTENTIAL

During iterations to self-consistency, the electron-electron repulsion energy is calculated from the effective interelectron electrostatic potential $V_{ee}(\vec{r})$, determined from the charge density of the previous iteration. With eigenvectors $\Psi_n(\vec{r})$ given by

$$\Psi_n(\vec{r}) = \sum_i C_i^n \chi_i(\vec{r}) , \tag{9}$$

where n denotes orbital and spin labels, the charge density is determined for the state specified by occupation numbers $\{f_k\}$,

$$n(\vec{r}) = \sum_k f_k \sum_{i,j} C_i^k C_j^k \chi_i(\vec{r}) \chi_j(\vec{r}) . \tag{10}$$

The evaluation of $V_{ee}(\vec{r})$ is typically the bottleneck in full-potential cluster calculations. In rydbergs,

$$V_{ee}(\vec{x})=2\int \frac{n(\vec{r})}{|\vec{r}-\vec{x}|}d\vec{r}\,. \tag{11}$$

In the present approach, potential evaluation is efficiently carried out in much the same way as described for the matrix elements. The density is partitioned into an all-Gaussian part by the extension of the orbital tails into their defining spheres, with correction components for the overcounted density inside the spheres. Explicitly,

$$V_{ee}(\vec{x})=2\sum_k f_k \sum_{i,j} C_i^k C_j^k \int \frac{\chi_i(\vec{r})\chi_j(\vec{r})}{|\vec{r}-\vec{x}|}d\vec{r}$$

$$=\sum_k f_k \sum_{i,j} C_i^k C_j^k v_{ij}(\vec{x})\,, \tag{12}$$

where

$$v_{ij}(\vec{x})=2\int \frac{\chi_i(\vec{r})\chi_j(\vec{r})}{|\vec{r}-\vec{x}|}d\vec{r}$$

$$=2\int \frac{G_i(\vec{r})G_j(\vec{r})}{|\vec{r}-\vec{x}|}d\vec{r}$$

$$+2\sum_k \int_{\Omega_k} \frac{\chi_i(\vec{r})\chi_j(\vec{r})-G_i(\vec{r})G_j(\vec{r})}{|\vec{r}-\vec{x}|}d\vec{r}\,. \tag{13}$$

The first integral on the right-hand side of Eq. (13) is treated by an adaptation of the McMurchie-Davidson algorithm for electron-nuclear matrix element evaluation.[11] The second term is a multicenter potential expansion due to the charge inside the atomic spheres. This density in a given sphere comes from the product of basis orbitals, at least one of which is defined on the given site, corrected for the extension of the corresponding orbital tail back into that site. If neither χ_i nor χ_j have their origin in sphere k, then the correction density in that site is seen to vanish. Combining Eqs. (12) and (13), the electron-electron Coulomb potential may be written

$$V_{ee}(\vec{x})=2\sum_n f_n \sum_{i,j} C_i^n C_j^n \int \frac{G_i(\vec{r})G_j(\vec{r})}{|\vec{r}-\vec{x}|}d\vec{r}+2\sum_k \int_{\Omega_k}\left[\sum_n f_n \sum_{i,j} C_i^n C_j^n \frac{\chi_i(\vec{r})\chi_j(\vec{r})-G_i(\vec{r})G_j(\vec{r})}{|\vec{r}-\vec{x}|}\right]d\vec{r}$$

$$=v_G(\vec{x})+\sum_k v_k(\vec{x})\,, \tag{14}$$

where $v_G(\vec{r})$ is the potential due to the Gaussians extended over all space and the contribution from sphere k is defined as

$$v_k(\vec{x})=2\int_{\Omega_k}\frac{n_k(\vec{r})}{|\vec{r}-\vec{x}|}d\vec{r}\,, \tag{15}$$

where

$$n_k(\vec{r})=\sum_n f_n \sum_{i,j} C_i^n C_j^n [\chi_i(\vec{r})\chi_j(\vec{r})-G_i(\vec{r})G_j(\vec{r})] \tag{16}$$

is the correction density in sphere k. Before evaluation of the potential due to this charge, the sharp structure in the core region is first diminished by subtracting from Eq. (16) (and adding back in separately) the density

$$n_0^k(r)=\frac{1}{4\pi}\sum_n a_n \int_{4\pi}(\Phi_n^2-G_n^2)d\Omega_k\,, \tag{17}$$

where the Φ_n and G_n are atomic basis components of $\{\chi\}$ defined in Eq. (2), and a_n are nominal atomic occupation numbers. This choice for $n_0^k(r)$ is readily seen to minimize the structure in the $l=0$ channel of

$$n_c^k(\vec{r})=n_k(\vec{r})-n_0^k(r) \tag{18}$$

and preserves the property that $n_c^k(\vec{r})\to 0$ as $r\to R_0^k$. A partial-wave decomposition of $n_c^k(\vec{r})$ is then carried out in each sphere and the corresponding electrostatic potential evaluated on a radial mesh of, typically, 10–40 points. That part of the spherical density subtracted out, $n_0^k(r)$, is treated separately with evalulation of the corresponding potential on a logarithmic radial mesh. The potential due to the density $n_c^k(\vec{r})$ can be expressed as a point multipole expansion for $r\geq R_0^k$,

$$v_k(\vec{r})=\sum_L Q_L^k Y_L(\hat{r})/r^{l+1}\,, \tag{19}$$

where Q_L^k is the L-multipole moment ($L=l,m$) of the reduced correction density given in Eq. (18).

V. ELECTRON-ELECTRON AND EXCHANGE-CORRELATION INTEGRAND SMOOTHING

A. Electron-electron matrix elements

With $V_{ee}(\vec{r})$ determined, the procedure for partitioning gives the matrix elements

$$V_{ij}^c=\langle G_i \mid V_{ee} \mid G_j\rangle_\infty$$

$$+\sum_k(\langle\chi_i \mid V_{ee} \mid \chi_j\rangle_{\Omega_k}-\langle G_i \mid V_{ee} \mid G_j\rangle_{\Omega_k})\,. \tag{20}$$

The magnitude of V_{ee} in the core region results in large contributions to the sphere matrix elements of Eq. (20). These are efficiently handled by evaluation of $l=0$ terms over a logarithmic radial mesh. While $V_{ee}(\vec{r})$ is smooth over Ω_I, the presence of large structure inside the spheres

also poses a problem with evaluation of the global matrix elements, Eq. (20). Integrand smoothing techniques[15] are usefully applied here by noting that the potential function V_{ee} in the global integrand of Eq. (20) can be modified at points inside the spheres as long as the modifications also enter the corrective second terms of the parentheses, which remove the overcounted interaction in the spheres. In particular, a fictitious slowly varying potential $\bar{V}_{ee}$ can be introduced, i.e.,

$$V_{ij}^{c}=\langle G_i \mid \bar{V}_{ee} \mid G_j \rangle_{\infty} + \sum_k (\langle \chi_i \mid V_{ee} \mid \chi_j \rangle_{\Omega_k} - \langle G_i \mid \bar{V}_{ee} \mid G_j \rangle_{\Omega_k}) \tag{21}$$

where

$$\bar{V}_{ee}(\vec{r})=\begin{cases} V_{ee}(\vec{r}), & \vec{r}\in\Omega_1 \\ V_{ee}(\vec{r}_k)-V_0(r_k)+V_G(r_k), & \vec{r}\in\Omega_k \end{cases} . \tag{22}$$

Here $V_0(r_k)$ denotes the $l=0$ component of $V_{ee}(\vec{r}_k)$ in sphere k. It is convenient to choose $V_G(r_k)$ as a combination of two Gaussians with coefficients chosen to match $V_0(r_k)$ smoothly at R_0^k. Then $\bar{V}_{ee}(\vec{r})$ is smooth over all space,[25] and the global integral is efficiently and accurately evaluated using Gaussian quadrature over a suitably defined coordinate system; in the two-center case, prolate spheriodal coordinates[26] are well suited.

B. Exchange-correlation matrix elements

The exchange-correlation potential[27] in the LSDA is given by

$$V_{\rm xc}(\vec{r})=\frac{\partial}{\partial n(\vec{r})}\{n(\vec{r})\epsilon_{\rm xc}[n(\vec{r})]\} . \tag{23}$$

The form of $V_{\rm xc}(\vec{r})$ is too complex for direct use of the Gaussian integral algorithms, and since $V_{\rm xc}(\vec{r})$ varies roughly as $n^{1/3}(\vec{r})$, rather large structure occurs in the core region. Again, the matrix element is partitioned:

$$V_{ij}^{\rm xc}=\langle G_i \mid V_{\rm xc} \mid G_j \rangle_{\infty} + \sum_k (\langle \chi_i \mid V_{\rm xc} \mid \chi_j \rangle_{\Omega_k} - \langle G_i \mid V_{\rm xc} \mid G_j \rangle_{\Omega_k}) . \tag{24}$$

Since in this case we are dealing with a local function of the density, it is most convenient to simply continue the Gaussian tails into their defining spheres (replacing the Φ representation) and use the resulting smooth density in Eq. (23) to define a fictitious potential, $\bar{V}_{\rm xc}$,

$$\bar{V}_{\rm xc}(\vec{r})=V_{\rm xc}[n_G(\vec{r})] , \tag{25}$$

where

$$n_G(\vec{r})=\sum_m f_m \sum_{i,j} C_i^m C_j^m G_i(\vec{r}) G_j(\vec{r}) . \tag{26}$$

Of course the real density $n(\vec{r})=n_G(\vec{r})$ for $\vec{r}$ in Ω_I, and $n_G(\vec{r})$ differs from $n(\vec{r})$ inside a given sphere in that the radial functions Φ_i for that site are replaced by the continuation of the Gaussian tails G_i into the sphere. Then the exchange-correlation matrix element with smoothing of the global integrand is

$$V_{ij}^{\rm xc}=\langle G_i \mid \bar{V}_{\rm xc} \mid G_j \rangle_{\infty} + \sum_k (\langle \chi_i \mid V_{\rm xc} \mid \chi_j \rangle_{\Omega_k} - \langle G_i \mid \bar{V}_{\rm xc} \mid G_j \rangle_{\Omega_k}) . \tag{27}$$

VI. TOTAL ENERGY CALCULATION

The solutions $\Psi_n^{\pm}(\vec{r})$ of the density functional single-particle equations are obtained by diagonalization of the secular matrix, and the majority $(+)$ and minority $(-)$ spin densities corresponding to the ground state are given by

$$n_{\pm}(\vec{r})=\sum_n f_n^{\pm} \mid \Psi_n^{\pm}(\vec{r}) \mid^2 , \tag{28}$$

where the $f_n^{\pm}$ are occupation numbers describing the state of interest. The total energy in the LSDA is given[27] (in rydbergs) by

$$E[n]=T_0[n]+\int n(\vec{r}) \left[\tfrac{1}{2} V_{ee}(\vec{r}) + \epsilon_{\rm xc}[n_+(\vec{r}),n_-(\vec{r})] - 2\sum_k \frac{Z_k}{\mid \vec{r}-\vec{R}_k \mid} \right] d\vec{r} + \sum_{i\neq j} \frac{Z_i Z_j}{R_{ij}} , \tag{29}$$

where the kinetic energy term is defined

$$T_0[n] \equiv -\sum_{s,n} f_n^s \langle \Psi_n^s \mid \nabla^2 \mid \Psi_n^s \rangle_{\infty} , \tag{30}$$

and $\epsilon_{\rm xc}(n_+,n_-)$ is the exchange-correlation energy density for a homogeneous spin-polarized electron gas of majority (minority) spin density n_+ (n_-).

The evaluation of the matrix elements of the Hamiltonian forms the essential part of the energy integral evaluation in the linear variational approach, and this has been described for all components of Eq. (29), except the term involving $\epsilon_{\rm xc}$. The latter is treated by extending the Gaussian tails into their defining sites and using the Gaussian density, Eq. (26), as the argument of $\epsilon_{\rm xc}$ in the global and correction integrals.

$$\begin{aligned} E_{\rm xc} &\equiv \int n(\vec{r}) \epsilon_{\rm xc}[n_+(\vec{r}),n_-(\vec{r})] d\vec{r} \\ &= \int n_G(\vec{r}) \epsilon_{\rm xc}[n_G^+(\vec{r}),n_G^-(\vec{r})] d\vec{r} \\ &\quad + \sum_k \int_{\Omega_k} \{ n(\vec{r}) \epsilon_{\rm xc}[n_+(\vec{r}),n_-(\vec{r})] - n_G(\vec{r}) \epsilon_{\rm xc}[n_G^+(r),n_G^-(\vec{r})] \} d\vec{r}_k . \end{aligned} \tag{31}$$

The kinetic energy, electron-nuclear energy, and electrostatic electron-electron energy components of $E[n]$, Eq. (29), are given in Appendix C.

VII. RESULTS

The class of systems for which this technique was devised involve transition-metal atoms. The copper dimer is a member of this class which is both well characterized experimentally and widely studied theoretically. The Cu_2 system has emerged as a benchmark for various theoretical techniques due to the relative simplicity of its bonding and the availability of a good experimental data base. Important for the present work is the existence of recent studies carried out within the LSDA.

As a test of procedures in this approach, components of the total energy were calculated with the segmented form of the AGB (see Appendix A) and compared with the same quantities in a separate LCGTO calculation using the same primitives (but without the augmentation step). This benchmark verified the procedures and established the level of accuracy of this approach to one part in 10^8 in energy. So the comparison with other works in the following serves as a more broad assessment of the general LCGTO method as applied to Cu_2.

Focus is placed on the ground state, but results are also given for some ionized and excited states of Cu_2. The question of the sensitivity of results in the LSDA to the specific form of exchange-correlation functional is also addressed. Calculations have been carried out using the Slater $X\alpha$ model[28] and the more recent functional of Vosko, Wilk, and Nusair[29] (VWN); some results using the earlier LSDA functional of Gunnarsson and Lundqvist[30] (GL) are also included.

The primitive Gaussian basis set used was derived from the $14s\,9p\,5d$ atomic basis set of Wachters[31] with limited extension and optimization of the most diffuse pair of s and p exponents and extension in the d channel by addition of the diffuse primitive suggested by Hay.[32] Solution of the LSDA equations for the copper atom $^2S(3d^{10}4s^1)$ state with all primitives free gave a total energy 0.0760 a.u. above the exact numerical $X\alpha$ result[33] (−1638.3304 a.u.), and the resulting eigenvector provided the linear coefficients for the minimal basis components in the contraction to $[14s\,11p\,6d/6s\,5p\,3d]$ form. Test calculations for the dimer including further freeing of primitive functions, modification of the most diffuse exponents, and addition of an f-polarization function established the convergence level of the $[14s\,11p6d/6s\,5p\,3d]$ basis at a few hundredths of an eV in binding energy. No frozen-core approximation was used; the AGB procedures for subtracting the atom density permit explicit core treatment with numerical convergence and stability to one part in 10^8.

A. Ground state of Cu_2

Self-consistent calculations for the $^1\Sigma_g^+$ ground state of Cu_2 were carried out for various internuclear separations. The curve of binding energies in the $X\alpha$ model is plotted as a function of bond length in Fig. 3. The associated spectroscopic constants are summarized along with results

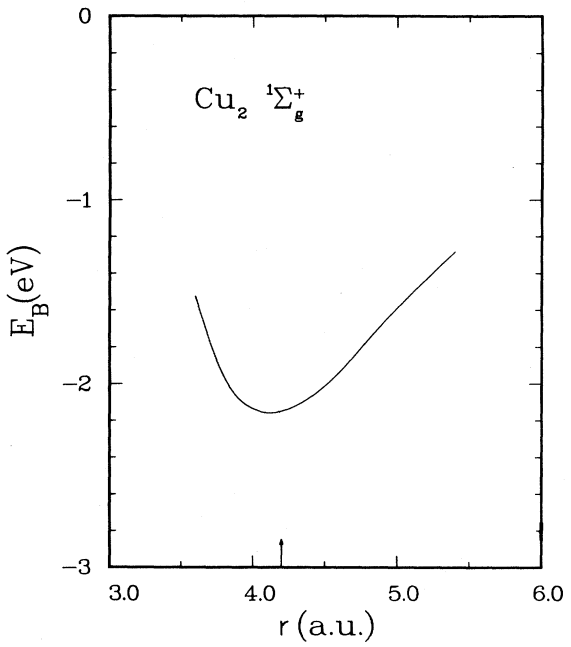

FIG. 3. Ground-state binding-energy curve for Cu_2 within the $X\alpha$ model. Arrow on abscissa denotes experimental bond length (4.20 a.u.).

from other LSDA works and compared with experiment[34] in Table I. The results for the $X\alpha$ model are in better overall agreement with experiment than are those for the more refined functionals. This signifies various types of errors in the atom and dimer are canceling.[35] The GL and VWN functionals (only the AGB-VWN results appear in Table I; AGB-GL results are almost identical) overbind more as a result of less complete error cancellation between atom and dimer. This characteristic, which is also reported for first-row molecules,[9,10,36–39] is discussed in some detail in Ref. 36. It is noted here that the total energy for the copper atom in the VWN model is approximately 0.57 a.u. further from experiment than that obtained in the GL model, consistent with the trend in the calculations of Wilk and Vosko.[40] The characteristic for LSDA vibrational frequencies to lie above experimentally observed values is also evident in Table I. Connected with

TABLE I. Comparison of various LSDA calculated spectroscopic constants for Cu_2. D_e, binding energy; R_e, equilibrium separation; and ω, vibrational frequency.

Calculation	D_e (eV)	R_e (a.u.)	ω (cm^{-1})
Experiment[a]	2.03	4.20	265
LMTO-GL[b]	2.30	4.31	280
AGB-VWN	2.65	4.10	330
AGB-$X\alpha$	2.16	4.12	290
LCAO-$X\alpha$-numerical[c]	2.10	4.20	286
LCAO-$X\alpha$-STO[c]	2.22	4.27	268

[a]Reference 34.
[b]Reference 46.
[c]Reference 47.

the tendency to overbind in the LSDA is the prediction in the AGB results of a bond length which is about 2% smaller than experiment.[34] This reduced bond length[41] is consistent with the reduced values for Wigner-Seitz radii found in LSDA calculations for crystals of the first-transition-metal series.[42] The large bond-length contraction which is observed at the CI level when $3d$ electrons are correlated[43] suggests that the characteristic energetic favoring of d electrons in the LSDA (Ref. 44) is the cause of the shortened bond length observed in the AGB results.[45] Relativistic effects have been estimated[43] to further contract the bond by approximately 0.13 a.u.

The AGB results with the GL functional are essentially the same as those with the VWN model. Differences with the spectroscopic constants in Harris and Jones's LCMTO results[46] are probably connected with limitations in the original LCMTO basis. For the $X\alpha$ model, the AGB- and LCAO-numerical orbital[47] results (Table I) agree in all quantities to better than 3%. Possible origins for the small differences are the smaller basis set and frozen-core approximation used in the LCAO work. The influence of basis incompleteness is well known, and the shifts associated with the frozen-core approximation[48] produce larger equilibrium separations than all-electron LSDA calculations. On the other hand, the special segmented form of the AGB used in this work can only be as complete as the full-Gaussian set of primitives from which it is constructed. To assess completeness with this form of the AGB, convergence studies were carried out by systematically freeing the most diffuse set of primitive Gaussians in s, p, and d channels, adding f orbitals, and varying exponents of the most diffuse tail orbitals. Results given in Table II establish the level of basis convergence in binding energy at a few hundredths of an electron volt. It is frequently the case in linear variational total-energy calculations for atomic clusters and solids[49] that the structural parameters are rather accurately predicted with a limited basis. In the AGB approach, minimal basis set calculations give an equilibrium separation R_e of approximately 4.16 a.u. (0.04 a.u. greater than the converged value),[50] although the binding energy is approximately 0.6 eV above the converged result.

TABLE II. Convergence of binding energy at $R=4.2$ a.u. with extension of augmented Gaussian basis set. Successive most diffuse primitive functions are denoted s,s',s'' in the $l=0$ channel; similarly for p, d, and f.

Basis	E_B (eV)
B[a]	−1.50
$B+s$	−1.57
$B+s+s'$	−1.61
$B+s+s'+p$	−1.72
$B+s+s'+p+p'$	−1.82
$B+s+s'+p+p'+d'$	−2.12
$B+s+s''+p+p''+d''$	−2.11
$B+s+s'+p+p'+d+d'$	−2.15
$B+s+s'+p+p'+d+d'+f$	−2.15

[a] B stands for the minimal basis set of occupied atomic orbitals for each site.

B. Description of bonding in Cu_2 within LSDA

Bonding in Cu_2 is traditionally pictured as involving a $4s$-$4s$ bond with the d orbitals filled and relatively inert. Bauschlicher *et al.*[43] have also emphasized the importance of $4s$ to $4p$ excitations in the CI framework. In the LSDA, moderate s-$d\sigma$ hybridization occurs. The AGB one-electron energy-correlation diagram for the dimer at equilibrium separation is given in Fig. 4. The spin-polarized atomic $3d$ and $4s$ states are observed to give rise to a singlet molecular state characterized by a low-lying $6\sigma_g$ level, primarily of $4s$ parentage, with a higher manifold of levels of mainly d origin (the lowest unoccupied level, $7\sigma_u$, lies above the scale of Fig. 4).

In Figs. 5–8, contour plots of the orbital density, $|\phi_i(\vec{r})|^2$ (in the x-z plane with atoms on the z axis), are given for each valence molecular level in the Cu_2 spectrum of Fig. 4. The bond densities correlate well with a simple description given by the one-electron-level structure. The orbital density of the $6\sigma_g$ level (Fig. 5) shows the maximum bond density between the sites (contour 9). This state is characterized by a strong bonding combination of s-s and $d\sigma$-$d\sigma$ molecular orbitals (eigenvector coefficients of symmetry orbitals of the $4s$, most diffuse free s, and $3d$ origin are ~0.5, 0.3, and 0.6, respectively). In the higher-energy manifold of levels of d-orbital parentage, the $3\pi_u$ is most stable. Although the $3\pi_u$ bond density in the plot plane is larger [contour 7 in Fig. 6(a)] than that of any other states in the d-bonding group, the magnitude is about five times smaller than the density at the bond center for the $6\sigma_g$ state. The δ-bonding state (Fig. 7) shows still less overlap density. Figures 6(b) and 7(b) show the antibonding states corresponding to the bonding orbitals in Figs. 6(a) and 7(a). The LSDA picture shows that both $d\pi$-$d\pi$ and $d\delta$-$d\delta$ bond densities are relatively weak in Cu_2 compared with that of s-s and $d\sigma$-$d\sigma$ bonds. But as is evident in Fig. 8, the bond density of the $7\sigma_g$ state [Fig. 8(a)] is quite weak. Orthogonality of this state

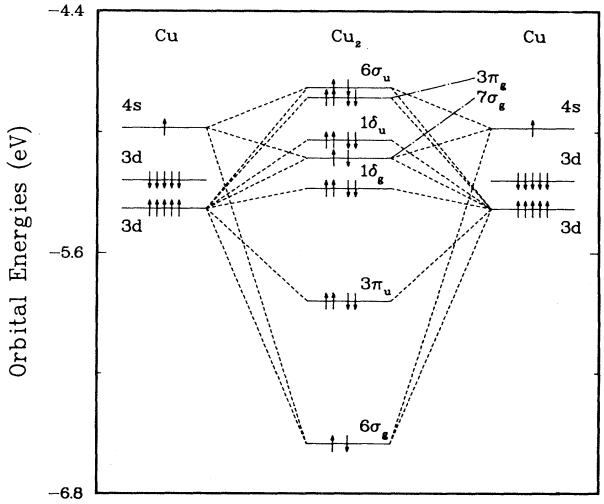

FIG. 4. Correlation diagram of one-electron energies for spin-polarized copper atom and Cu_2 with atoms at equilibrium separation.

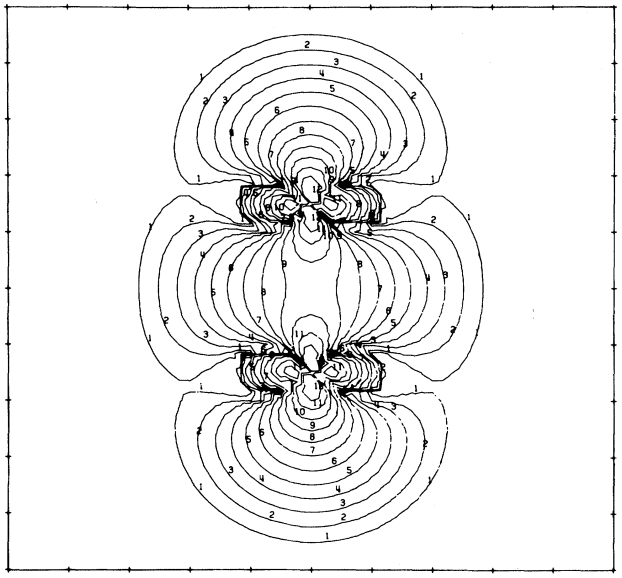

FIG. 5. Contour plot of orbital density, $|\psi(\vec{r})|^2$, for $6\sigma_g$ state of Cu_2 at equilibrium separation. The plane intersects atoms, and adjacent contours differ by a factor of 2, with initial value $=0.0001$ (contour 1).

to the $6\sigma_g$ results in a destructive superposition between the s-s and the $d\sigma$-$d\sigma$ bonding molecular orbital components reducing the bond density along the internuclear axis. The resulting orbital density of the $7\sigma_g$ state is much like a hollow toroid with reduced $d_{3z^2-r^2}$ lobes at the atom sites aligned along its axis [Fig. 8(a)]. The highest occupied state, $6\sigma_u$, is characterized as a simple antibonding combination of $d_{3z^2-r^2}$ orbitals on each site [Fig. 8(b)]. To summarize, the picture of bonding in Cu_2 within the LSDA is one of s-s and $d\sigma$-$d\sigma$ hybridized bonds providing the major stability in Cu_2 with weaker contributions from $d\pi$-$d\pi$ and $d\delta$-$d\delta$ bonds. Intercomparison of the orbital-force components of the Hellmann-Feynman force also indicates the $6\sigma_g$ density is the major contributor, however, all valence-orbital forces are attractive at equilibrium separation and fall in the range of approximately 1.5—2.7 hartree/bohr.

C. Ionized and excited states of Cu_2

Calculations within the LSDA for states above the ground state of a given symmetry are formally beyond the regime of applicability of density-functional theory, however, experience shows the errors are often reasonably small. Relaxation within the LSDA can also be influenced by the removal of symmetry restrictions,[51] but for this study, symmetry equivalence of the copper sites is assumed ($D_{\infty h}$ symmetry). First it should be noted that the $X\alpha$ model with $\alpha=0.7$ already provides accurate first and second ionization potentials (IP) for the copper atom. Total energy separations between states of Cu^n and Cu^{n+1} ($n=0,1$), as calculated with several LSDA models, are compared with expeirment[52] in Table III. At least for this typical value of α, the simpler scaled exchange-correlation

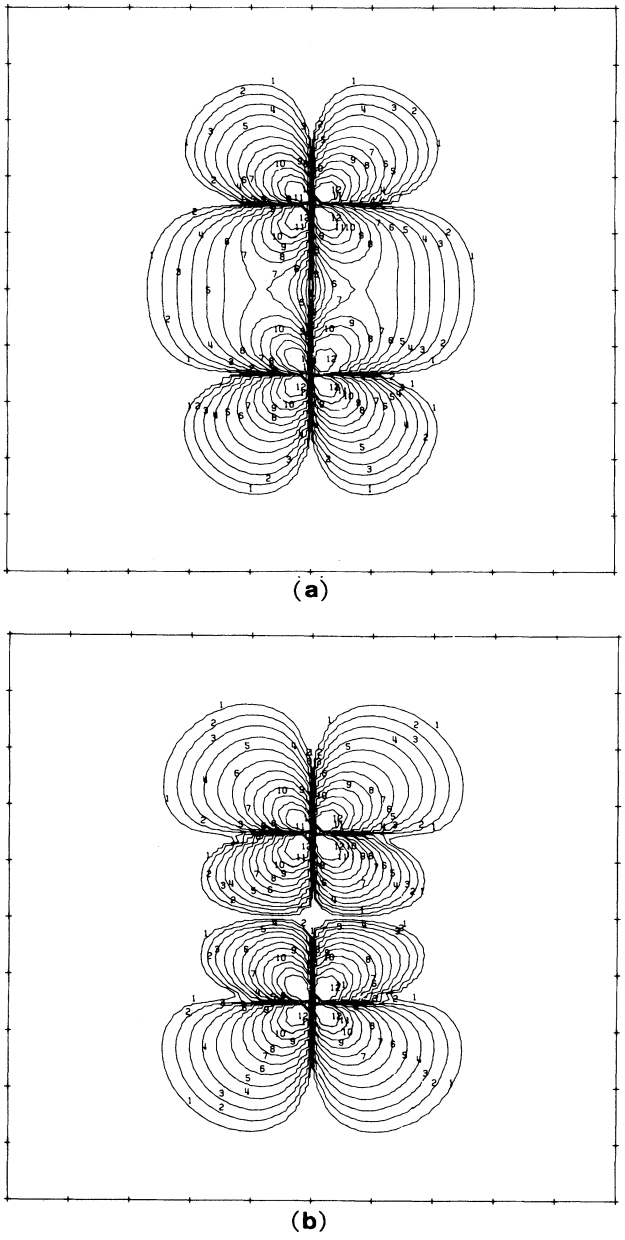

FIG. 6. Orbital density contours of (a) $3\pi_u$ and (b) $3\pi_g$ molecular orbitals of Cu_2. Degenerate components normal to the plane also exist. Contour values are as given for Fig. 5.

approximation of the $X\alpha$ model gives more accurate atomic-ionization energies than the more detailed LSDA functionals of GL and VWN.[53]

Within the LSDA, the highest occupied state according to orbital energy is the $6\sigma_u$ which is predominantly d-like (Fig. 8). The energy of Cu_2^+ ($^2\Sigma_u^+$) produced by removing one electron from this state is not the lowest ionized state however; the latter is obtained by ionizing a $7\sigma_g$ electron to give a $^2\Sigma_g^+$ Cu_2^+ state. Energy differences calculated for these states are compared with experiment in Table IV. The VWN and GL models overestimate the first IP by 1.1—1.3 eV while the $X\alpha$ results is within approximate-

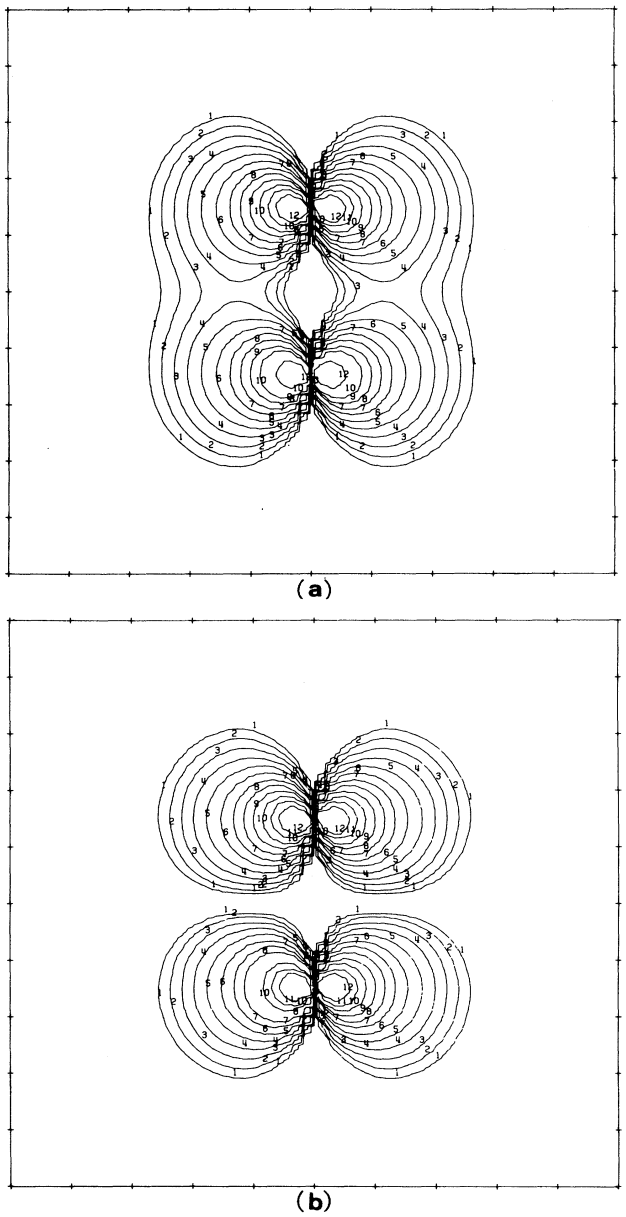

FIG. 7. Orbital density contours of the (a) $1\delta_g$ and (b) $1\delta_u$ states of Cu_2. Each has a degenerate component for which the plot plane is a nodal surface. Contour values are same as for Fig. 5.

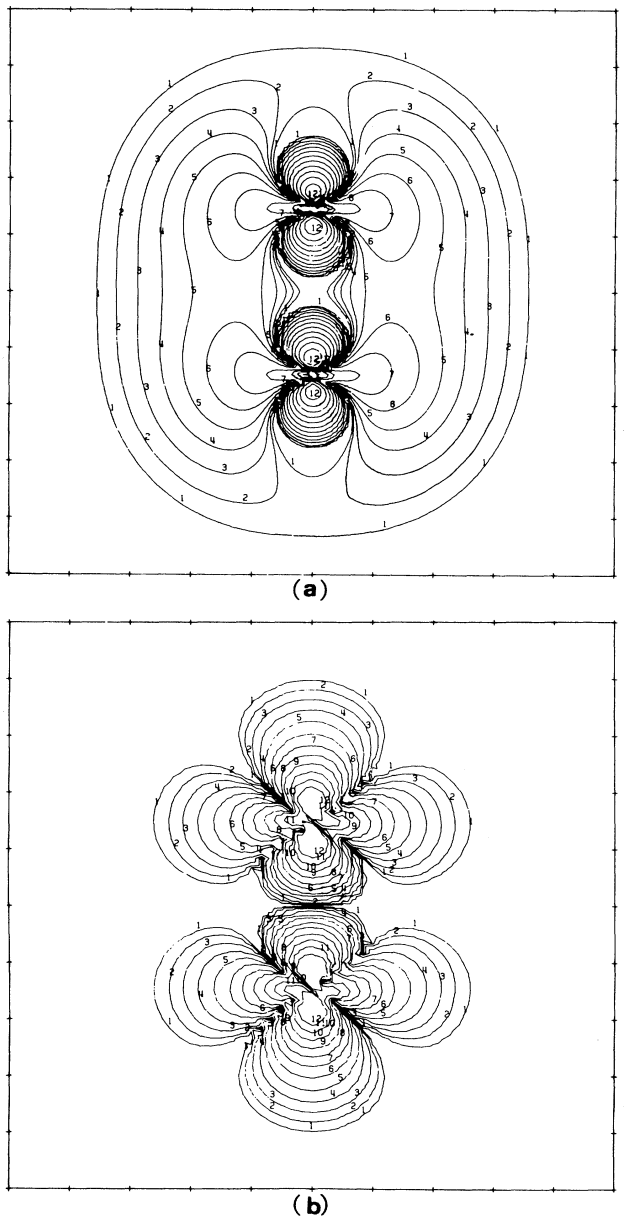

FIG. 8. Orbital density contours of the (a) $7\sigma_g$ and (b) $6\sigma_u$ states of Cu_2. Contour values are same as noted in Fig. 5.

ly 0.15 eV of experiment. From the study of Post and Baerends,[51] ionization from the $7\sigma_g$ level to produce the $^2\Sigma_g^+$ state is not affected by symmetry breaking so the corresponding results in Table IV should be reliable. However, the $6\sigma_u$ ionization energy is reported[51] to increase by approximately 1.8 eV. This shift would place the $^2\Sigma_u^+$ state of Table IV well in excess of the first ionization potential.

In Table V excitation energies for symmetry-allowed transitions $7\sigma_g^{\uparrow} \rightarrow 7\sigma_u^{\uparrow}$ and $3\pi_g^{\uparrow} \rightarrow 7\sigma_u^{\uparrow}$ are summarized for AGB calculations using the $X\alpha$ and VWN functionals.

TABLE III. First and second ionization potentials (IP) of copper atom calculated within $X\alpha$, GL, and VWN models using the AGB approach. Experimental data from Moore.[a]

	First IP (eV)	Second IP (eV)
Experiment[a]	7.72	20.21
$X\alpha$	7.73	20.70
VWN	8.35	21.64
GL	8.58	21.99

[a]Reference 52.

TABLE IV. Ionized state energies (in eV) of Cu_2 relative to $^1\Sigma_g^+$ ground state calculated within the $X\alpha$, GL, and VWN models. Experimental[a] first IP equals 7.37 eV.

Cu_2^+ state	$^2\Sigma_g^+$	$^2\Sigma_u^+$
$X\alpha$	7.52	8.34
VWN	8.45	9.24
GL	8.67	9.55

[a]Reference 34.

Experimentally, two close-lying excited states are observed at approximately 2.54 and 2.60 eV above the ground state.[54] The VWN results are in better agreement with experiment than the $X\alpha$ model in this case; however, the separation of the two states is too large ($\sim$0.2 eV) for both functionals. The lower-energy transition, which in this work is associated with states that are predominantly *s*-like, is not expected to be influenced much by symmetry breaking, however, the $3\pi_g^\uparrow \rightarrow 7\sigma_u^\uparrow$ transition, involving an initial state with large atomic *d* character, is reported to be significantly affected in Hartree-Fock calculations.[55]

VIII. SUMMARY

The calculations carried out for Cu_2 confirm the expected advantages of the AGB approach, viz., (a) high accuracy and efficiency in the calculation of the electron-electron electrostatic matrix elements, and (b) reduced storage requirements and computation times stemming from the reduction in the number of Gaussian functions to a few diffuse orbital tails.[56] These advantages are achieved while maintaining the principal desirable characteristic of the Gaussian-type basis, i.e., the use of integral formulas for valence-orbital tail interactions. The replacement of core Gaussians by numerical radial functions allows further improvement in the description of the inner-sphere part of the wave function. In the alternate mode of using a full-Gaussian basis in a segmented manner, by partitioning into compact and diffuse (tail) segments, basis convergence typical of all-Gaussian (LCGTO) schemes is obtained. However, as only the orbital tail functions enter the calculation as Gaussians (the remainder being treated as numerical functions), the full calculational advantages of the augmentation procedure apply.

The results obtained for Cu_2 using different model exchange-correlation functionals show that the Slater scaled-exchange $X\alpha$ model gives a more accurate description of ground-state spectroscopic constants than recent functionals with more accurate descriptions of the correlation energy in the LSDA. The $X\alpha$ model even gives a better first ionization potential for the dimer (as it does for the copper atom); for excitation energies of Cu_2, it is somewhat less accurate than the VWN model. Binding energies for first-row dimers to the right of Be_2 similarly show closer agreement with experiment in the $X\alpha$ model,[11] but it is observed that the predictions within this functional are less systematic from member to member in the series.

TABLE V. Excitation energies of Cu_2 calculated within the $X\alpha$ and VWN models. Assignment of excitations taken from calculation.

Excitation	$(7\sigma_g^\uparrow \rightarrow 7\sigma_u^\uparrow)$	$(3\pi_g^\uparrow \rightarrow 7\sigma_u^\uparrow)$
Experiment[a]	2.54	2.60
$X\alpha$	2.12	2.30
VWN	2.31	2.50

[a]Reference 54.

The results of the AGB calculation suggest that the LSDA predicted bond length of Cu_2 is 2% shorter than experiment. This finding differs from the results of other calculations, but it is consistent with the reduced lattice constant found in bulk LSDA calculations.

A number of extensions of the AGB approach can be carried out to achieve even further efficiencies. Among them, the incorporation of developments to eliminate explicit treatment of the core[57] appears most promising.

ACKNOWLEDGMENT

This research was sponsored by the Division of Materials Sciences, U.S. Department of Energy under Contract No. W-7405-eng-26 with the Union Carbide Corporation.

APPENDIX A: SEGMENTED GAUSSIAN BASIS SET

It is possible to cast full-Gaussian expansions of atomic orbitals into the AGB form if members of the basis are separated into compact and diffuse sets. The AGB procedures then can be directly used. This not only permits a useful contact with existing calculations employing full-Gaussian basis sets, but also provides valuable internal consistency checks between quantities calculated numerically and by formula. In a full-Gaussian basis, an atomic radial function can be written

$$\phi(r)=r^l\left[\sum_{i=1}^{N_c} c_i \exp(-\alpha_i r^2) + \sum_{i=1}^{N_d} d_i \exp(-\beta_i r^2)\right], \tag{A1}$$

where there are N_c "compact" Gaussians, characterized by $\alpha_i \geq \alpha_c \equiv -\ln(\tau/R_0^l)/R_0^2$ and N_d "diffuse" Gaussians with $\beta_i < \alpha_c$. The critical exponent value[58] α_c depends upon the parameter τ defining the tolerance for vanishing of the Gaussians at the sphere radius R_0. If the full expansion Eq. (A1) is identified with $\phi(r)$ of Eq. (2), and the diffuse set in Eq. (A1) with the tail function in Eq. (1), it is clear that the AGB form is attained. The compact set of Gaussians is treated just as the numerical form of ϕ, so that the large number of primitives is effectively reduced to the much smaller set of diffuse Gaussians, thus removing a major limitation in the LCGTO method.

The basis composed of functions of this form can be described as a "segmented" Gaussian basis, but it should not be confused with the segmentation introduced in some *ab initio* work.[1] The segmented form of the AGB is obviously not as accurate for the core region, or for the isolated atom case where the numerical solutions are exact

within the LSDA framework. In the context of the present study, however, the cross checks afforded by this form were deemed so important to establishing the accuracy of the method that the segmented form of the AGB was used. The present approach was verified by comparison of results from minimal basis set calculations for Cu_2 using the segmented AGB with results from calculations using the same set of primitive Gaussians without the augmentation procedure. The agreement in total energies was to millirydberg accuracy.

APPENDIX B: MATRIX ELEMENTS

Some matrix elements for which Gaussian global integral algorithms[11] are used include overlap

$$\langle \chi_i \mid \chi_j \rangle_\infty = \langle G_i \mid G_j \rangle_\infty + \sum_k (\langle \chi_i \mid \chi_j \rangle_{\Omega_k} - \langle G_i \mid G_j \rangle_{\Omega_k}) , \tag{B1}$$

electron-nuclear

$$\left\langle \chi_i \left| \sum_m \frac{Z_m}{\mid \vec{r}-\vec{R}_m \mid} \right| \chi_j \right\rangle_\infty = \sum_m Z_m \left[\langle G_i \mid \mid \vec{r}-\vec{R}_m \mid^{-1} \mid G_j \rangle_\infty - \sum_k (\langle \chi_i \mid \mid \vec{r}-\vec{R}_m \mid^{-1} \mid \chi_j \rangle_{\Omega_k} - \langle G_i \mid \mid \vec{r}-\vec{R}_m \mid^{-1} \mid G_j \rangle_{\Omega_k}) \right] , \tag{B2}$$

and kinetic energy

$$-\tfrac{1}{2}\langle \chi_i \mid \nabla^2 \mid \chi_j \rangle_\infty = -\frac{1}{2} \left[\langle G_i \mid \nabla^2 \mid G_j \rangle_\infty + \sum_k (\langle \chi_i \mid \nabla^2 \mid \chi_j \rangle_{\Omega_k} - \langle G_i \mid \nabla^2 \mid G_j \rangle_{\Omega_k}) \right] . \tag{B3}$$

APPENDIX C: ENERGY EXPRESSIONS

1. Kinetic energy

We have

$$T_0[n] = -\sum_{s,n} f_n^s \langle \Psi_n^s \mid \nabla^2 \mid \Psi_n^s \rangle_\infty \tag{C1}$$

$$= -\sum_{s,n} f_n^s \sum_{i,j} C_i^{ns} C_j^{ns} \langle \chi_i \mid \nabla^2 \mid \chi_j \rangle_\infty \tag{C2}$$

$$= -\sum_{s,n} f_n^s \sum_{i,j} C_i^{ns} C_j^{ns} \left[\langle G_i \mid \nabla^2 \mid G_j \rangle_\infty + \sum_k (\langle \chi_i \mid \nabla^2 \mid \chi_j \rangle_{\Omega_k} - \langle G_i \mid \nabla^2 \mid G_j \rangle_{\Omega_k}) \right] . \tag{C3}$$

The global integral in Eq. (C3) is evaluated using the algorithms of McMurchie and Davidson,[11] and the remaining terms are calculated by standard procedures for the sphere.

2. Electron-nuclear energy

We have

$$E_{Ne} \equiv -2 \int n(\vec{r}) \sum_m \frac{Z_m}{\mid \vec{r}-\vec{R}_m \mid} d\vec{r} \tag{C4}$$

$$= -2 \sum_{s,n} f_n^s \sum_{i,j} C_i^{ns} C_j^{ns} \sum_m Z_m \int \frac{\chi_i \chi_j}{\mid \vec{r}-\vec{R}_m \mid} d\vec{r} \tag{C5}$$

$$= -2 \sum_{s,n} f_n^s \sum_{i,j} C_i^{ns} C_j^{ns} \left[\sum_m Z_m \int \frac{G_i G_j}{\mid \vec{r}-\vec{R}_m \mid} d\vec{r} + \sum_k \int_{\Omega_k} (\chi_i \chi_j - G_i G_j) \sum_m \frac{Z_m}{\mid \vec{r}-\vec{R}_m \mid} d\vec{r} \right] . \tag{C6}$$

The global integration over the extended tails is carried out using Gaussian integral algorithms[11] and the sphere integrations involving the correction density interacting with the nuclear electrostatic potential are carried out numerically.

3. Electron-electron electrostatic energy

We have

$$E_{es} \equiv \tfrac{1}{2} \int n(\vec{r}) V_{ee}(\vec{r}) d\vec{r} \tag{C7}$$

$$= \tfrac{1}{2} \sum_{s,n} f_n^s \sum_{i,j} C_i^{ns} C_j^{ns} \int \chi_i V_{ee}(\vec{r}) \chi_j d\vec{r} \tag{C8}$$

$$= \tfrac{1}{2} \sum_{s,n} f_n^s \sum_{i,j} C_i^{ns} C_j^{ns} V_{ij}^c \ , \tag{C9}$$

where V_{ij}^c, the electron-electron matrix element, is given in Eq. (21).

---

*Permanent address: Judson College, Elgin, IL 60120.

[1]T. H. Dunning and P. J. Hay, in *Modern Theoretical Chemistry, Methods of Electronic Structure Theory,* edited by H. F. Schaefer III (Plenum, New York, 1977), Vol. 3, Chap. 1, pp. 1–27.

[2]H. Tatewaki and S. Huzinaga, J. Chem. Phys. 71, 4339 (1979).

[3]Y. Sakai, H. Tatewaki, and S. Huzinaga, J. Comp. Chem. 3, 6 (1982).

[4]M. Pelissier, J. Chem. Phys. 75, 775 (1981).

[5]For a review of LSDA calculations, see A. R. Williams and U. von Barth, in *Theory of the Inhomogeneous Electron Gas,* edited by S. Lundqvist and N. H. March (Plenum, New York, 1983).

[6]R. C. Chaney, T. K. Tung, C. C. Lin, and E. E. Lafon, J. Chem. Phys. 52, 361 (1970).

[7]P. J. Feibelman, J. A. Appelbaum, and D. R. Hamann, Phys. Rev. B 20, 1433 (1979); J. G. Harrison, C. C. Lin, and W. Y. Ching, *ibid.* 24, 6060 (1981); J. W. Mintmire, J. R. Sabin, and S. B. Trickey, *ibid.* 26, 1743 (1982); J. Callaway, Xianwu Zou, and D. Bagayoko, *ibid.* 27, 631 (1983).

[8]H. Sambe and R. H. Felton, J. Chem. Phys. 61, 3862 (1974); 62, 1122 (1975).

[9]B. I. Dunlap, J. W. D. Connolly, and J. R. Sabin, J. Chem. Phys. 71, 3396 (1979); 71, 4993 (1979); J. W. Mintmire and B. I. Dunlap, Phys. Rev. A 25, 88 (1982).

[10]G. S. Painter and F. W. Averill, Phys. Rev. B 26, 1781 (1982).

[11]L. E. McMurchie and E. R. Davidson, J. Comp. Phys. 26, 218 (1978).

[12]B. Delley and D. E. Ellis, J. Chem. Phys. 76, 1949 (1982).

[13]O. K. Andersen and R. G. Woolley, Mol. Phys. 26, 905 (1973).

[14]For a review see H. L. Skriver, *The LMTO Method* (Springer, New York, 1983).

[15]J. Harris and G. S. Painter, Phys. Rev. B 22, 2614 (1980).

[16]J. Harris, R. O. Jones, and J. E. Mueller, J. Chem. Phys. 75, 3904 (1981), and references therein.

[17]F. Casula and F. Herman, J. Chem. Phys. 78, 858 (1983).

[18]J. C. Slater, Phys. Rev. 51, 846 (1937).

[19]A. R. Williams, J. Kuebler, and C. D. Gelatt, Jr., Phys. Rev. B 19, 6094 (1979).

[20]I. P. Batra, A. R. Williams, K. C. Pandey, and J. F. Janak, Bull. Am. Phys. Soc. 26, 206 (1981).

[21]R. C. Raffenetti, J. Chem. Phys. 58, 4452 (1973).

[22]A projection of the spherical average of the potential about a site can be produced at any iteration and outward integration of the radial differential equation for some prescribed energy ϵ_i defines $\phi(\epsilon_i, r)$. In the simplest form of this method, the energies are the atomic eigenvalues of the isolated atoms, so that core solutions are exact and the basis set is complete at large separation.

[23]For discussion purposes the Gaussian expansion is written in spherical harmonic form, but in practice Cartesian Gaussian functions are used (see Ref. 11).

[24]The AGB approach can be simply extended to treat functions matched at other sites, and energy derivative components can be included. The present choice of orbitals is made as the simplest extension of the usual LCGTO method.

[25]Compared with the integrand smoothing procedure used in the LCMTO approach (Ref. 15), there is no need to introduce a match function for the tail orbital G since it automatically has the desired smooth behavior inside the spheres.

[26]A. N. Lowan, in *Handbook of Mathematical Functions,* edited by M. Abramowitz and I. R. Stegun (National Bureau of Standards, Washington, D.C., 1972).

[27]W. Kohn and L. J. Sham, Phys. Rev. 140, A1133 (1965).

[28]J. C. Slater, *Quantum Theory of Molecules and Solids* (McGraw-Hill, New York, 1973), Vol. IV.

[29]S. H. Vosko, L. Wilk, and M. Nusair, Can. J. Phys. 58, 1200 (1980).

[30]O. Gunnarsson and B. I. Lundqvist, Phys. Rev. B 13, 4274 (1976); see also O. Gunnarsson, J. Appl. Phys. 49, 1399 (1978).

[31]A. J. H. Wachters, J. Chem. Phys. 52, 1033 (1970).

[32]P. J. Hay, J. Chem. Phys. 66, 4377 (1977).

[33]The numerical energy in the Hartree-Fock limit is -1638.9642 a.u. (Ref. 32) which is 0.6338 a.u. *lower* than the $X\alpha$ total energy with $\alpha = 0.7$. The other functionals studied here are similarly above the Hatree-Fock result, indicating the dominance of exchange error in present forms of the LSDA.

[34]K. P. Huber and G. L. Herzberg, *Molecular Spectra and Molecular Structure. IV. Constants of Diatomic Molecules* (Van Nostrand Reinhold, New York, 1979).

[35]The $X\alpha$ model typically works better for energy separations involving low-spin states; characteristically, the scaled-exchange approximation to correlation energy density overemphasizes the stability of high-spin states.

[36]G. S. Painter, Phys. Rev. B 24, 4264 (1981).

[37]R. O. Jones, J. Chem. Phys. 76, 3098 (1982).

[38]E. J. Baerends and P. Ros, Int. J. Quantum. Chem. Symp. 12, 169 (1978).

[39]J. E. Mueller, R. O. Jones, and J. Harris, J. Chem. Phys. 79, 1874 (1983).

[40]L. Wilk and S. H. Vosko, J. Phys. C 15, 2139 (1982).

[41]It should be emphasized that whereas the variational principle applies to the exact model ground-state energy corresponding to the functional in use, the value of the minimum may lie *lower* than the exact ground-state energy of the physical system, and the exact values of associated spectroscopic constants do not form bounds for those of the model system. Thus, for example, bond lengths within the LSDA may be calculated (exactly) which are smaller than observed values. This contrasts with many-electron treatments in which calculated bond lengths typically lie above physically observed values if basis set superposition error is eliminated.

[42]V. L. Moruzzi, J. F. Janak, and A. R. Williams, *Calculated Electronic Properties of Metals* (Pergamon, New York, 1978).
[43]C. W. Bauschlicher, Jr., S. P. Walch, and P. E. M. Siegbahn, J. Chem. Phys. 76, 6015 (1982).
[44]O. Gunnarsson and R. O. Jones, Phys. Scr. 21, 394 (1980).
[45]Basis-set superposition error (see Ref. 55), which can also lead to bond shortening, is considered to be a negligible factor in the AGB calculations from the observed stability of results with respect to basis changes. It is noted that for rather broad minima, as in the case of Cu_2, internal numerical stability and the reduction of R-dependent inaccuracies in binding energies to a level below 0.01 eV over 0.1 a.u. is required.
[46]J. Harris and R. O. Jones, J. Chem. Phys. 70, 830 (1979).
[47]B. Delley, D. E. Ellis, A. J. Freeman, E. J. Baerends, and D. Post, Phys. Rev. B 27, 2132 (1983).
[48]U. von Barth, Phys. Rev. A 20, 1693 (1979).
[49]M. Weinert, E. Wimmer, and A. J. Freeman, Phys. Rev. B 26, 4571 (1982).
[50]Similar shifts in lattice constant are quoted in Ref. 49. See also C. Bachmann, J. Demuynck, and A. Veillard, Faraday Symp. Chem. Soc. 14, 170 (1980).
[51]D. Post and E. J. Baerends, Chem. Phys. Lett. 86, 176 (1982).
[52]C. E. Moore, Natl. Stand. Ref. Data Ser. Natl. Bur. Stand. 34, 6c (1970).
[53]The GL and VWN model erros in ionization potential given in Table III are about 0.1 eV smaller than those reported for manganese by Wilk and Vosko (Ref. 40).
[54]R. M. Steele, J. Mol. Spectrosc. 61, 477 (1976).
[55]E. Miyoshi, H. Tatewaki, and T. Nakamura, J. Chem. Phys. 78, 815 (1983).
[56]Evaluation of the Coulomb potential due to the Gaussian tails extended over all space [$v_G(\vec{x})$ in Eq. (14)] forms the rate-determining step in the LSDA approach with Gaussian functions, in the absence of density and potential fit procedures. This step goes as MN^2, where M is the number of points at which the potential is required and N is the number of Gaussian functions. Since only the diffuse Gaussians representing the orbital tails enter the AGB (on average, a third the number in a full-Gaussian basis), an order of magnitude reduction in both the computation time and storage requirements for components of $v_G(\vec{x})$ is effected.
[57]See, for example, discussion of core-projected self-consistent-field theory by J. C. Malvido and J. L. Whitten, Phys. Rev. B 26, 4458 (1982).
[58]R. N. Euwema, Phys. Rev. B 4, 4332 (1971).